Arabsalmani, M, Roychowdhury, S, Renaud, F, Cormier, D, Le Floc'h, E, Emsellem, E, Perley, DA, Zwaan, MA, Bournaud, F, Arumugam, V and Moller, P

A Superluminous Supernova in High Surface Density Molecular Gas within the Bar of a Metal-rich Galaxy

The Astrophysical Journal, 882:31 (7pp), 2019 September 1 https://doi.org/10.3847/1538-4357/ab2897

A Superluminous Supernova in High Surface Density Molecular Gas within the Bar of a Metal-rich Galaxy

M. Arabsalmani[1,2,3], S. Roychowdhury[4,5], F. Renaud[6], D. Cormier[3], E. Le Floc'h[3], E. Emsellem[7], D. A. Perley[8], M. A. Zwaan[7], F. Bournaud[3], V. Arumugam[7], and P. Møller[7]
[1] School of Physics, University of Melbourne, Parkville, VIC 3010, Australia; maryam.arabsalmani@unimelb.edu.au
[2] ARC Centre of Excellence for All Sky Astrophysics in 3 Dimensions (ASTRO 3D), Australia
[3] IRFU, CEA, Université Paris-Saclay, F-91191 Gif-sur-Yvette, France
[4] Centre for Astrophysics and Supercomputing, Swinburne University of Technology, Hawthorn, VIC 3122, Australia
[5] Institut d'Astrophysique Spatiale, CNRS, Université Paris-Sud, Université Paris-Saclay, Bât. 121, F-91405 Orsay Cedex, France
[6] Department of Astronomy and Theoretical Physics, Lund Observatory, Box 43, SE-221 00 Lund, Sweden
[7] European Southern Observatory, Karl-Schwarzschildstrasse 2, D-85748 Garching Bei Muenchen, Germany
[8] Astrophysics Research Institute, Liverpool John Moores University, 146 Brownlow Hill, Liverpool L3 5RF, UK
Received 2019 April 22; revised 2019 May 31; accepted 2019 June 3; published 2019 August 28

Abstract

We report the Atacama Large Millimeter/submillimeter Array observations of the metal-rich host galaxy of superluminous supernova (SLSN) PTF10tpz, a barred spiral galaxy at $z = 0.03994$. We find the CO(1–0) emission to be confined within the bar of the galaxy. The distribution and kinematics of molecular gas in the host galaxy resemble gas flows along two lanes running from the tips of the bar toward the galaxy center. These gas lanes end in a gaseous structure in the inner region of the galaxy, likely associated with an inner Lindblad resonance. The interaction between the large-scale gas flows in the bar and the gas in the inner region plausibly leads to the formation of massive molecular clouds and consequently massive clusters. This in turn can result in formation of massive stars, and thus the likely progenitor of the SLSN in a young, massive cluster. This picture is consistent with SLSN PTF10tpz being located near the intersection regions of the gas lanes and the inner structure. It is also supported by the high molecular gas surface densities that we find in the vicinity of the SLSN, surface densities that are comparable with those in interacting galaxies or starburst regions in nearby galaxies. Our findings therefore suggest in situ formation of massive stars due to the internal dynamics of the host galaxy and also lend support to high densities being favorable conditions for formation of SLSN progenitors.

Key words: galaxies: ISM – ISM: kinematics and dynamics – ISM: molecules – submillimeter: galaxies – supernovae: individual (SLSN PTF10tpz)

1. Introduction

Superluminous supernovae (SLSNe) are rare and extremely bright transients (Smith et al. 2007; Quimby et al. 2013). Their luminous emission remains brighter than the peak magnitude of most supernovae (SNe) for hundreds of days. Their peak visual absolute magnitudes are 10–100 times brighter than those of typical core-collapse SNe (e.g., Quimby et al. 2011), making it possible to detect them at $z > 2$ (Cooke et al. 2012; Curtin et al. 2019). To date, the underlying explosion mechanism behind these recently identified energetic events remains speculative. However, their very large energy releases suggest that they arise from the stars at the very high mass end of the stellar initial mass function with $M \gtrsim 100\,M_{\odot}$ (Gal-Yam & Leonard 2009). Studying the close environments of SLSNe can provide valuable insights into understanding the physical conditions in which their progenitors form, and thus put constraints on progenitor models for their formation.

Similarly to the conventional classification of SNe according to their spectroscopic properties, SLSNe are grouped into two main subclasses: hydrogen-poor events (SLSN-I), and events with spectroscopic signatures of hydrogen (SLSN-II; see Gal-Yam 2012). Both groups appear to trace the ultraviolet light of their host galaxies, which supports the association between their progenitors and massive stars (Neill et al. 2011; Lunnan et al. 2015). Their hosts are found to be mainly irregular, compact, dwarf galaxies, with high star formation rate (SFR) surface densities, and high specific star formation rates (Lunnan et al. 2013, 2014, 2015; Angus et al. 2016; Perley et al. 2016). Although, the host galaxies of type II SLSNe seem to cover a larger range in galaxy masses and metallicities compared to type I SLSN hosts (Neill et al. 2011; Angus et al. 2016; Perley et al. 2016).

The typical low metallicity of SLSN hosts could imply a strong metallicity bias for SLSN progenitors (Lunnan et al. 2014; Perley et al. 2016; Chen et al. 2017), favoring single-star progenitor models with low mass loss due to stellar winds (Langer et al. 2007). However the detection of a fraction of SLSNe (of both types) in quite large, massive, and metal-rich host galaxies raises questions about whether low metallicity is indeed necessary for the formation of SLSN progenitors (see Lunnan et al. 2015; Perley et al. 2016; Nicholl et al. 2017; Bose et al. 2018). In some of the metal-rich cases, the location of the SLSN is coincident with the central regions—the most metal-rich regions of the host galaxy (Gal-Yam 2012). A more likely, but less addressed, factor is the formation of SLSN progenitor stars in dense environments. Massive stars are more likely to be found in massive star clusters that form in dense giant molecular clouds (GMCs). This picture is consistent with the occurrence of SLSNe in the central regions of metal-rich galaxies as gas flows, driven by galaxy interactions or bars, can create dense concentrations of molecular gas in the central regions of galaxies (Sheth et al. 2005; Gallagher et al. 2018). It is also compatible with progenitor models in which massive stars in dense and young star cluster merge into a star with sufficient mass for forming an SLSN (Portegies Zwart & van

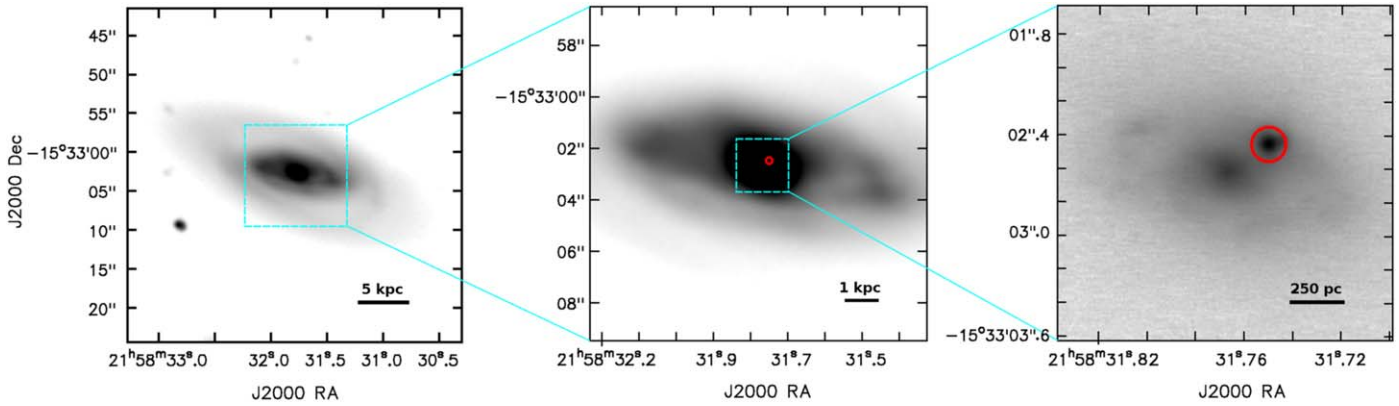

Figure 1. Left and middle panels: the *R*-band image of SLSN PTF10tpz host galaxy obtained by Keck/LRIS showing the presence of a bar along with spiral-like structures in the galaxy. The cyan squares show the area covered in the panel immediately to the right. Right panel: the *K*-band adaptive optics image of the central 1.5 kpc of the host galaxy at the time when SLSN PTF10tpz was bright. The red circles in the middle and right panels mark the location of the SLSN with a radius indicating the uncertainties on the SLSN coordinates.

den Heuvel 2007; Pan et al. 2012; van den Heuvel & Portegies Zwart 2013).

SLSN PTF10tpz (type II SLSN) at $z = 0.03994$ is one of the SLSNe that occurred close to the nucleus of a massive and metal-rich galaxy. In this paper we study the properties of molecular gas, the fuel for star formation, in the close environment of this SLSN, and investigate whether its progenitor is formed in a dense environment. We present deep carbon monoxide (CO) emission line observations of the host galaxy of SLSN PTF10tpz obtained by Atacama Large Millimeter/submillimeter Array (ALMA). The high spatial and spectral resolution of our ALMA observations and the fairly close distance of the host galaxy (183 Mpc using a flat ΛCDM with cosmological parameters from Planck Collaboration et al. 2018) allow us to model the dynamics of gas in the galaxy and to investigate the conditions in which the SLSN progenitor formed. This is the first study of molecular gas in an SLSN host galaxy.

2. Observations and Data Analysis

We used the Band-3 receivers of the ALMA 12 m Array in C43-6 configuration to map the CO(1–0) emission of the host galaxy on 2018 January 4 (project code: 2017.1.01568.S; PI: Arabsalmani). The observations used a 2 GHz band, centered on 110.883 GHz, covering the redshifted CO(1–0) emission line. This band was subdivided into 1920 channels, yielding a velocity resolution of $\sim$2.6 km s^{-1}, and a total velocity coverage of about 5400 km s^{-1}. The initial calibration of the data is done by the ALMA support staff, using the ALMA data pipeline in the COMMON ASTRONOMY SOFTWARE APPLICATIONS (CASA) package (McMullin et al. 2007). We use the CASA package TCLEAN to produce a spectral cube with a velocity resolution of $\sim$16 km s^{-1}. With Natural weighting, we yield a synthesized beam size of $0\farcs36 \times 0\farcs52$, and an rms noise of 0.3 mJy per channel in the cube.

We create a secondary data cube from our spectral data cube by applying Hanning smoothing across blocks of three consecutive velocity channels (using the CASA-SPECSMOOTH task), followed by spatial smoothing by convolving with a Gaussian kernel of FWHM equal to 6 pixels (using the CASA-IMSMOOTH task). The smoothing ensures that any localized noise peaks are ignored and only emission correlated spatially and in velocity is chosen. We then mask out pixels in the original spectral data cube that lie below a threshold flux in the secondary data cube. The threshold flux used to select pixels is approximately twice the noise in a line-free channel of the original spectral data cube. We obtain the total intensity and the intensity-weighted velocity field maps of the CO(1–0) emission line by applying the IMMOMENT tasks in CASA package on the original spectral data cube with masked pixels.

We also use a *R*-band image of SLSN PTF10tpz host galaxy presented in Perley et al. (2016). This image was obtained on 2011 November 26 by the Low-Resolution Imaging Spectrometer (LRIS; Oke et al. 1995) on the Keck I 10 m telescope (Program PI: S. Kulkarni, proposal ID: C219LA). We fit elliptical isophotes to the optical image using the STSDAS package in IRAF, and find the observed axial ratios of outermost isophotes converge to be 0.42. This yields an inclination angle of 68° for the optical disk of the galaxy assuming a typical intrinsic axial ratio of 0.2 for the stellar disk.

We use archival data of the observations of PTF10tpz with the Near-Infrared Camera on Keck II (NIRC2) in adaptive optics mode on UT 2010 October 29 between 06:01 and 06:56 UT (Program PI: A. Boden; proposal ID: C246N2L) in order to establish the location of PTF10tpz. Five dithered exposures were acquired in each of the *J*, *H*, and *K*′ filters. Each exposure consisted of 5 × 30 s coadds in *H* and *K*′ and 8 × 30 s coadds in *J*. A basic reduction with NIR sky subtraction and coaddition of dithered frames is performed. We measure the astrometric offset of PTF10tpz relative to the galaxy nucleus to be $0\farcs25 \pm 0\farcs01$ W and $0\farcs16 \pm 0\farcs01$ N, relying on the telescope orientation keywords in the header.

3. Results and Discussion

The Keck/LRIS *R*-band image of the host galaxy of SLSN PTF10tpz is shown in the left and middle panels of Figure 1. A bright stellar bar in the center of the galaxy, along with a faint spiral-like structure suggest that the host is an SB-type galaxy (see Table 1 for the global properties of the host). The right panel of Figure 1 shows the inner region of the galaxy at the time when the SLSN PTF10tpz was bright. We find the CO(1–0) emission to be confined within the stellar bar of the host galaxy, and extending over a projected physical size of $\sim$10 kpc. The emission has a W_{20} of 470 km s^{-1} and is centered at a redshift of $z = 0.03976 \pm 0.00007$. The maps of the total intensity and the intensity-weighted velocity field of

Table 1
Global Properties of the Host Galaxy of SLSN PTF10tpz

R.A. (J2000)	Decl. (J2000)	Redshift	$12+\log_{10}[O/H]$	M_* ($M_\odot$)	$(S\Delta v)_{CO(1-0)}$ (Jy km s^{-1})	$W_{20,\,CO(1-0)}$ (km s^{-1})	M_{mol} ($M_\odot$)
21:58:31.77	−15:33:02.61	0.03976 ± 0.00007	9.22	$10^{10.85}$	(18.39 ± 0.32)	470	$10^{9.8}$

Note. Columns 1 and 2: the coordinates of the galaxy center obtained from the Keck/LRIS image. Column 3: the redshift of the galaxy measured from the CO(1–0) emission line. Columns 4 and 5: the metallicity and stellar mass from Perley et al. (2016). Columns 6 and 7: the velocity-integrated flux density and the W_{20} of the CO(1–0) emission line. Column 8: the molecular gas mass of the host galaxy.

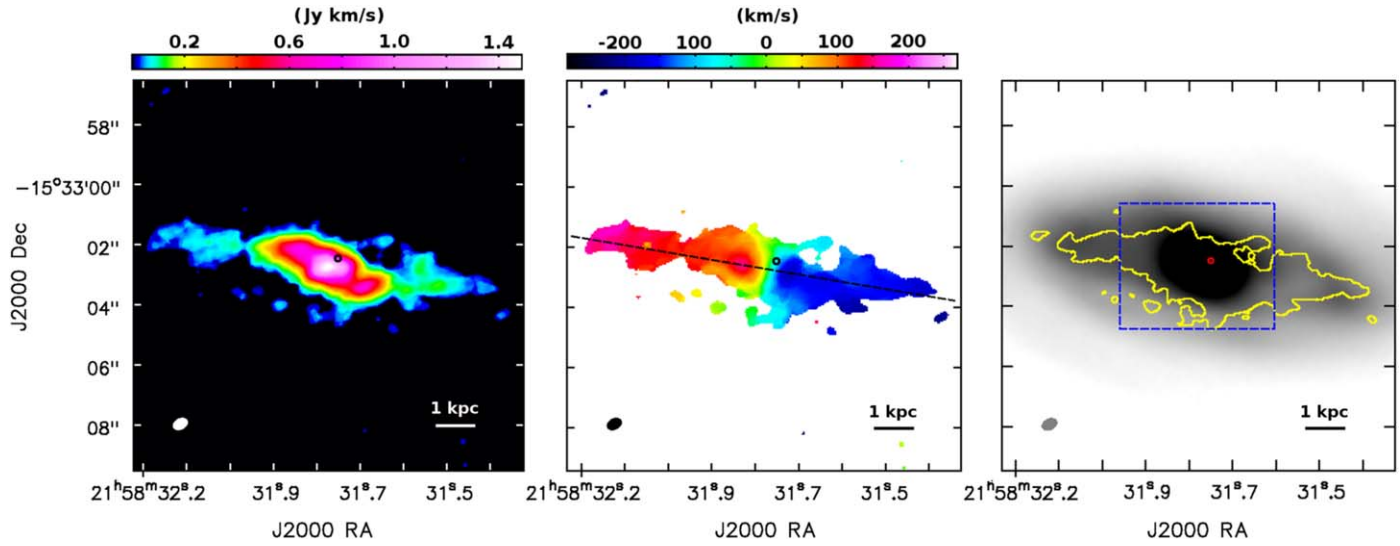

Figure 2. Left panel: the total intensity map of the CO(1–0) emission line in the host galaxy of SLSN PTF10tpz. The color bar is the flux density of CO(1–0) emission line. Middle panel: the intensity-weighted velocity field of the CO(1–0) emission line corresponding to the left panel. The color bar is the velocity with respect to the center of the CO(1–0) emission (at $z = 0.03976$). Right panel: the R-band image of the galaxy bar in the same frame as the other two panels, and also the middle panel of Figure 1. The yellow contour marks the extent of the CO(1–0) emission at 5σ significance. The dashed blue box shows the area covered in the channel maps presented in Figure 3. In all panels the synthesized beam is marked in the bottom left corner, and the position of the SLSN is marked with a circle. The radius of the circle indicates the uncertainties on the SLSN coordinates.

the CO(1–0) emission line are shown in the left and middle panels of Figure 2, respectively. The right panel of Figure 2 shows the R-band image of the galaxy bar within the same frame as in the left and the middle panels (also, the same frame as in the middle panel of Figure 1).

From the total intensity map it is clear that the CO emission has a significant contribution from the inner regions. Specifically, the central 1 kpc of the galaxy appears to contain about 25% of the total flux of the CO(1–0) emission. The intensity-weighted velocity field of the CO(1–0) emission line is reminiscent of a rotating structure with a distinct fast rotation in the central 1 kpc of the galaxy. Notably, the molecular gas in this inner region extends over >500 km s^{-1} in velocity space.

We measure a velocity-integrated flux density of 18.39 ± 0.32 Jy km s^{-1} over a total velocity range of 570 km s^{-1}, for the CO(1–0) emission from the galaxy. This implies a brightness temperature luminosity (as defined in Obreschkow et al. 2009) of $L'_{CO(1-0)} = (1.45 \pm 0.03) \times 10^9$ K km s^{-1} pc^2. We assume a Galactic CO-to-molecular-gas conversion factor of $\alpha_{CO} = 4.36\,M_\odot$(K km s^{-1} pc^2)$^{-1}$, based on the supersolar metallicity of the host (Perley et al. 2016) and obtain a molecular gas mass of $10^{9.8}\,M_\odot$ for the host galaxy. With the stellar mass of $10^{10.85}\,M_\odot$ (Perley et al. 2016), this yields a molecular gas mass-to-stellar mass ratio of ∼0.1 for the SLSN host, typical of nearby star-forming galaxies with similar stellar masses (Bothwell et al. 2014). We note that the conversion factor in the central kiloparsec of nearby galaxies is found to be a factor of 2 lower than the mean value (Sandstrom et al. 2013). Since a significant fraction of the CO emission is from the central few kiloparsecs of the host galaxy, its molecular gas mass could be lower by a factor of 2. However, for consistency and to compare our results with the literature we use the molecular gas mass estimated by assuming a Galactic conversion factor. This does not affect our conclusions.

Perley et al. (2016) performed spectroscopic observations for the host galaxy using a 1″ slit passing through the galaxy center along its major axis and measured the fluxes of the bright emission lines in the central regions of the galaxy (within the 1″ slit). They performed a BPT diagram analysis using the log [O III/Hβ] versus log([N II]/Hα] diagram and found the emission line fluxes to be consistent with the presence of an active galactic nucleus (AGN) in the galaxy center. They reported an average Hα-based SFR of $6.0\,M_\odot$ yr^{-1} for the central regions of the host and stated this to be an upper limit due to a (subdominant) contribution from the AGN to the Hα flux. However, we note that the host galaxy on the log[OIII/Hβ] versus log([NII]/Hα] plane lies in a region that is at the border between the AGN and star-forming galaxy regimes, and hence it is hard to confirm or rule out the presence of an AGN based on this diagram. On the other hand, the fluxes of the S[II] lines reported by Perley et al. (2016) place the host galaxy among the star-forming galaxies on the log[OIII/Hβ] versus log([SII]/Hα] plane (see Kewley et al. 2006; Singh et al. 2013).

We therefore use the $6.0\,M_{\odot}\,\mathrm{yr}^{-1}$ as the reference value for the SFR in the central regions of the galaxy. By measuring the molecular gas mass in the same region we estimate an average molecular-gas-depletion time (M_{mol}/SFR) of 0.7 Gyr, similar to depletion times in nearby starburst galaxies (see, e.g., Bigiel et al. 2008).

We obtain a mean molecular gas surface density of $\Sigma_{\mathrm{mol}} \sim 160\,M_{\odot}\,\mathrm{pc}^{-2}$ for the galaxy, averaged over the area within which CO(1–0) emission is detected (as defined based on the total intensity map) and corrected for the inclination of the host. This is comparable with the mean molecular gas surface densities of starburst galaxies in the local universe (also determined by averaging within the radius of the central molecular disk as determined from their CO maps; see Kennicutt 1998). In order to investigate the nature of the high mean surface density of the host, we measure the molecular gas surface densities over individual beams, or equivalently over ∼350 pc scales. We find these to be as high as $\sim 1400\,M_{\odot}\,\mathrm{pc}^{-2}$ in the inner region of the galaxy. In particular, we measure a Σ_{mol} of $\sim 700\,M_{\odot}\,\mathrm{pc}^{-2}$ over a beam centered on the SLSN location. These values are larger or comparable to the molecular gas surface densities obtained for the central regions of strongly barred nearby galaxies over smaller scales (e.g., 120 pc scales; Sun et al. 2018). We use the molecular gas clumping factors from Leroy et al. (2013) to convert the surface densities averaged over the scales probed by a single beam to the surface densities on the scale of individual clouds (∼50 pc). We predict the GMCs in the inner region of the host galaxy to have surface densities as high as $\sim$5000–10,000 $M_{\odot}\,\mathrm{pc}^{-2}$. These are comparable with the surface densities of GMCs in the Antennae galaxy or the nuclear starburst of NGC 253 (Leroy et al. 2015; Sun et al. 2018). The high molecular gas surface densities in the vicinity of the SLSN supports the hypotheses in which high densities are favorable conditions for formation of SLSNe progenitors (see also Arabsalmani et al. 2015, 2019; Roychowdhury et al. 2019).

We investigate the kinematics and structure of molecular gas using channel maps of the CO(1–0) emission at $16\,\mathrm{km\,s}^{-1}$ velocity resolution presented in Figure 3. These maps cover the inner region of the bar. The two white ellipses, following the orientation and flattening of the outermost isophotes of the disk, are there to help follow the path of the emission through the velocity channels. The CO emission is mainly concentrated along the path traced by these two ellipses. The emission coincident with the outer ellipse is confined mainly to the top left and bottom right quadrants of the ellipse. This emission extends beyond the frame covered in the channel maps in several channels, forming the faint extended wings that can be seen in the left panel of Figure 2. The emission coincident with the inner ellipse on the other hand is mainly restricted to the top right and bottom left quadrants of the ellipse, and is present in all channels with velocities between $-250\,\mathrm{km\,s}^{-1}$ and $257\,\mathrm{km\,s}^{-1}$. This emission forms a steep profile in the position–velocity (P–V) diagram of the CO(1–0) emission (Figure 4), making an X-shape pattern when combined with the emission from the outer structure (see Bureau & Freeman 1999; Merrifield & Kuijken 1999).

The spatial distribution and kinematics of the molecular gas shown in Figures 2 and 3 are consistent with the presence of two gas lanes, running from the tips of the bar toward the galaxy center. The specific orbital structures imposed by the bar and the dissipative nature of the gas lead to two symmetric well-defined gas lanes, often associated with shocks (see, e.g., Maciejewski et al. 2002; Emsellem et al. 2015). Figure 5 shows a simple sketch of such structures in the bar of the host galaxy of SLSN PTF10tpz. In this picture, the innermost parts of the two gas lanes encounter an inner Lindblad resonance associated with the pattern speed of the bar, close to the location of the SLSN. The transition of gas from the gas lanes to the inner resonance results in the formation of high-density gas with large velocity dispersions. This in turn leads to the formation of large GMCs at the intersection of the gas lanes and the inner resonance (similar to what is seen in NGC 1365; Elmegreen et al. 2009). The Keck/NIRC2 *Kp*-band image of the inner region of the host (the right panel of Figure 1) suggests the presence of a stellar ring with similar dimensions as those of the inner ellipse in Figure 3. With a semimajor axis of about 0.1 times the length of the bar, the size of this ring is consistent with the observed median value of 0.11 for the ratio of the nuclear ring size to the bar size in the catalog of Comerón et al. (2010). This lends support to the association of the molecular gas in the inner region of the galaxy with a resonance ring. Nuclear rings are common in spiral bar galaxies, and are shown to be the sites of intense starbursts where massive and compact star clusters can form (Elmegreen 1994; Benedict et al. 2002; Elmegreen et al. 2009; Combes et al. 2013). Note that deeper observations with higher spatial resolutions are required in order to precisely determine the location of the resonance. The existing observations do not provide enough information on the pattern speed of the bar, the epicycle frequency, and the mass distribution, to allow a detailed dynamical modeling of the galaxy.

Although the spatial resolution of data presented here does not allow us to reveal the exact nature of the inner structure of molecular gas in the host galaxy, it is likely that the interaction between the large-scale gas flows in the bar and the gas in the inner region has led to cloud–flow or cloud–cloud collisions. Observations and simulations show that cloud–cloud collisions lead to the assembly of giant molecular complexes, and consequently to the formation of massive star cluster(s) (e.g., Inoue & Fukui 2013). This is accompanied by an increase in the SFR (e.g., Tan 2000), and even a decrease in the depletion time (Renaud et al. 2015), similar to starbursts, like those typically hosted by interacting galaxies. In addition, it has been proposed that cloud–cloud collisions trigger the formation of massive stars (Motte et al. 2014; Takahira et al. 2018).

All these, together with the high molecular gas surface densities and short depletion time we report, suggest that massive clusters have formed near the intersection regions of the gas lanes and the inner structure that we have identified in the host galaxy of SLSN PTF10tpz. Such clusters are the birthplace of massive stars, potential progenitors of SLSNe, either directly and/or through a runaway process in their core (Portegies Zwart & van den Heuvel 2007; Pan et al. 2012; van den Heuvel & Portegies Zwart 2013). These clusters would then continue their motion along the ring (clockwise in Figure 5), which is compatible with the location of the SLSN (see Figures 3 and 5). The orbital velocity along the ring together with the separation between the formation and explosion sites of the SLSN progenitor can provide constraints on the lifetime and thus the mass of the progenitor star.

In order to have a rough estimate for the mass of the progenitor star we assume the orbital velocity along the ring to be same as the radial velocity at the apocenters of the inner

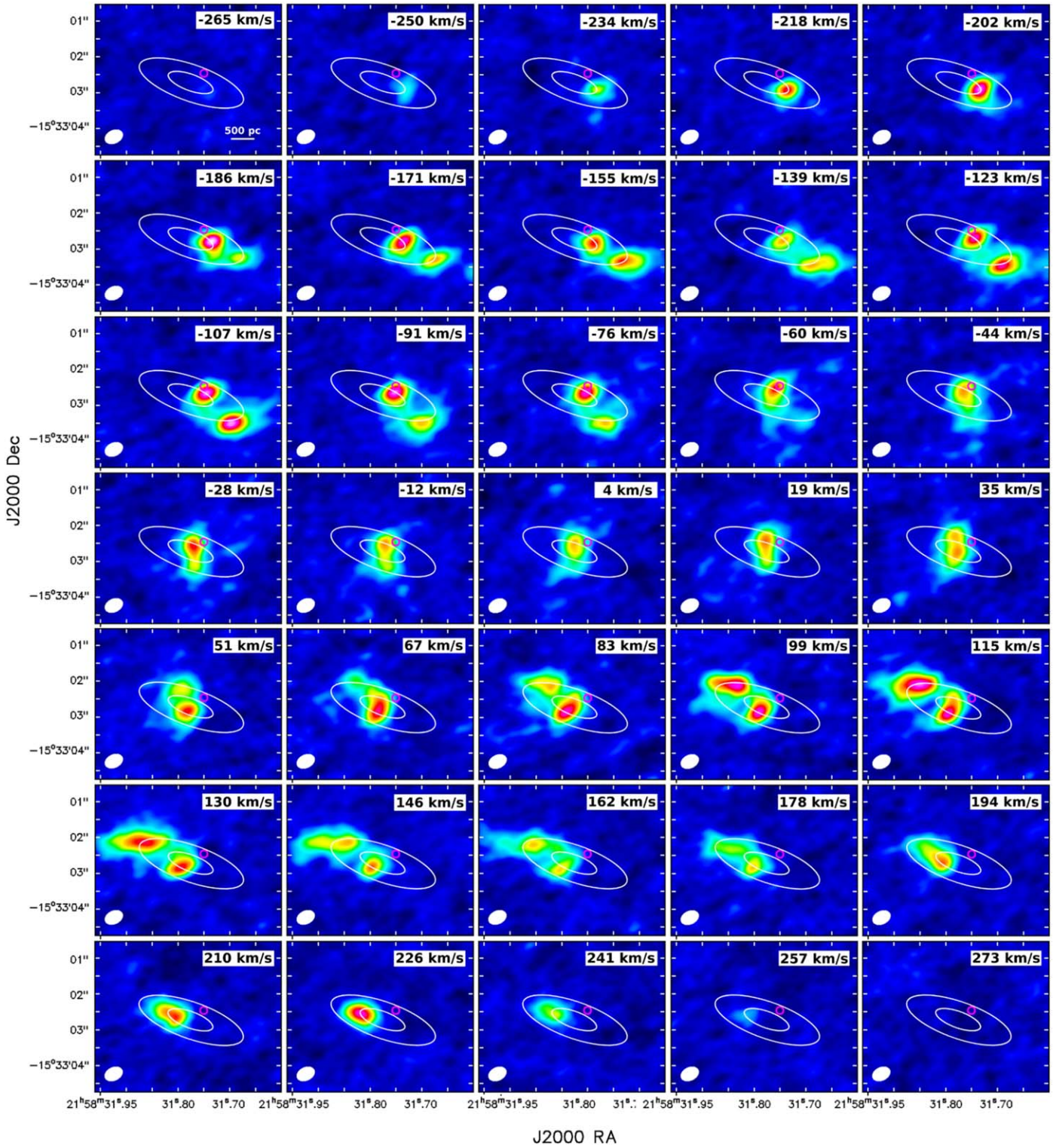

Figure 3. CO emission flux in successive 16 km s^{-1} velocity channels. Each map covers the area marked with the dashed blue box in the right panel of Figure 2. The two white ellipses are there to help follow the path of the emission through the velocity channels, within the central few kiloparsecs of the galaxy. The orientations and axial ratios of the two ellipses are same as those of the outermost isophotes of the optical disk of the galaxy. The position of the SLSN is marked with a magenta circle with a radius indicating the uncertainties on the SLSN coordinates. The beam is shown in the bottom left corner of each panel.

ellipse in Figure 3, i.e., about 250 km s^{-1}. If the progenitor star was indeed formed at the intersection of the gas lanes and the inner structure, it would have an age of about 3 Myr when it reached the explosion site. This would predict a stellar mass of $\sim$100 $M_{\odot}$ for the SLSN progenitor star (see Leitherer et al. 1999; Crowther et al. 2010). It is, however, likely that a delay, of the order of a few times the freefall time, exists between the assembly of the dense cloud at this intersection and the formation of the star itself. For a surface density of a few thousands $M_{\odot}$ pc^{-2} on the scale of individual molecular clouds, we estimate a volume density of $\sim$50 $M_{\odot}$ pc^{-3} and thus a freefall time of $\sim$1 Myr. Considering this delay, the estimated

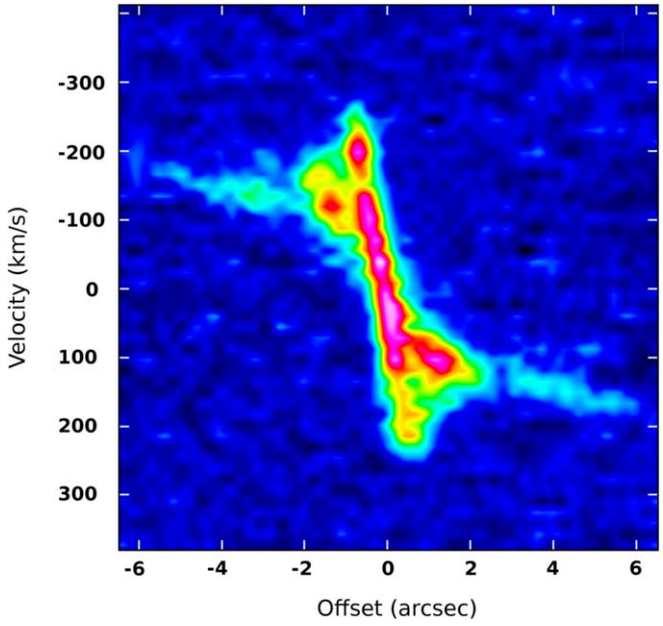

Figure 4. *P–V* diagram of the CO(1–0) emission where the position varies along the main rotation axis of the CO emission (the dashed black line in the middle panel of Figure 2).

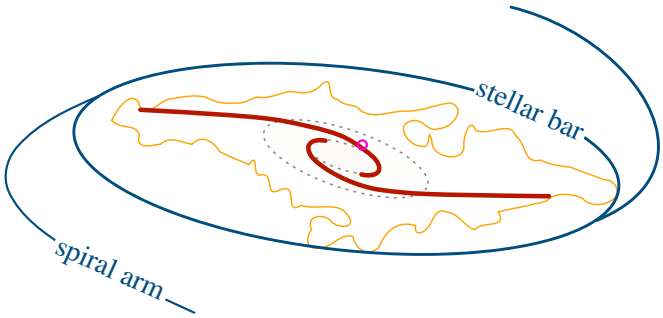

Figure 5. Sketch of the central structures in the host galaxy of SLSN PTF10tpz. The blue ellipse shows the stellar bar of the galaxy. The orange contour shows the extent of the molecular gas in the bar, as presented in the right panel of Figure 2. The two dotted gray ellipses represent the two ellipses in Figure 3. The two red spirals show the gas lanes along which the molecular gas flows toward the galaxy center. The position of the SLSN is marked by a magenta circle.

100 $M_\odot$ is in fact a lower limit for the mass of the SLSN progenitor star. The uncertainty on the progenitor mass dominantly comes from the mass–lifetime relation of very massive stars. The theoretical models for this relation suffer from substantial uncertainties, in particular due to dependency on parameters such as the spin and the metallicity of the star and also the internal mixing (e.g., Decressin et al. 2007). However, according to our current knowledge and state-of-the-art models, timescales of the order of 1–2 Myr correspond to the most massive stars known (see, e.g., Köhler et al. 2015). The very short timescale that we estimate between the onset of formation and the explosion of the progenitor star ($\lesssim$1 Myr) therefore indicates that the progenitor star of SLSN PTTF10tpz is among the most massive stars.

4. Summary and Conclusions

We study the spatial distribution and kinematics of molecular gas in the metal-rich and barred host galaxy of SLSN PTF10tpz though CO(1–0) emission line observations with ALMA. We detect the CO(1–0) emission line within the bar of the galaxy. The molecular gas in the inner region of the bar, where the SLSN is located, has surface densities as high as $\sim$1400 $M_\odot$ pc^{-2} at $\sim$350 pc scales. This predicts surface densities of $\sim$5000 $-$ 10,000 $M_\odot$ pc^{-2} for individual GMCs, comparable with those of GMCs in the Antennae galaxy or the starburst regions in the nearby universe. We find the distribution and kinematics of gas to be consistent with two gas lanes running from the tips of the bar toward the galaxy center. These lanes encounter a gaseous structure in the central $\sim$1 kpc of the galaxy. The position of SLSN PTF10tpz is very close to the the intersection regions of the gas lanes and the inner structure. This structure is plausibly associated with an inner Lindblad resonance ring, also suggested by the Keck/NIRC2 image of the inner region of the host. It is likely that the interaction between the large-scale gas flows in the bar and the gas at the inner resonance leads to the assembly of giant molecular complexes, and consequently to the formation of massive star clusters. This is supported by the short depletion time and high surface densities of molecular gas that we measure in the central regions of the galaxy. Our findings therefore suggest in situ formation of massive star clusters (in one of which the SLSN progenitor was formed) due to the internal dynamics of the host galaxy and without any external contribution such as interaction or merger. This demonstrates the important role that the kiloparsec-scale (hydro)dynamics of galaxies could play in the formation of massive stars and hence massive star explosions.

We would like to thank Nissim Kanekar for valuable contributions to this project. We thank Robert Quimby, Andy Boden, and Gaspard Duchesne for triggering and acquiring the Keck/NIRC2 observations. Many thanks to Ariane Lancon and Fabrice Martins for valuable insights on the lifetime of massive stars. We also thank Peter Erwin for helpful discussions. M.A. acknowledges support from the Australian Research Council Centre of Excellence for All Sky Astrophysics in 3 Dimensions (ASTRO 3D) through project number CE170100013. F.R. acknowledges support from the Knut and Alice Wallenberg Foundation. D.C. is supported by the European Union's Horizon 2020 research and innovation programme under the Marie Skłodowska-Curie grant agreement No 702622. ALMA is a partnership of ESO (representing its member states), NSF (USA) and NINS (Japan), together with NRC (Canada), NSC and ASIAA (Taiwan), and KASI (Republic of Korea), in cooperation with the Republic of Chile. The Joint ALMA Observatory is operated by ESO, AUI/NRAO and NAOJ.

ORCID iDs

M. Arabsalmani https://orcid.org/0000-0001-7680-509X
S. Roychowdhury https://orcid.org/0000-0002-5820-4589
D. Cormier https://orcid.org/0000-0002-1046-2685
E. Emsellem https://orcid.org/0000-0002-6155-7166
D. A. Perley https://orcid.org/0000-0001-8472-1996
M. A. Zwaan https://orcid.org/0000-0003-0101-1804
F. Bournaud https://orcid.org/0000-0002-5743-0250
P. Møller https://orcid.org/0000-0002-9994-505X

References

Angus, C. R., Levan, A. J., Perley, D. A., et al. 2016, MNRAS, 458, 84
Arabsalmani, M., Roychowdhury, S., Starkenburg, T. K., et al. 2019, MNRAS, 485, 5411

Arabsalmani, M., Roychowdhury, S., Zwaan, M. A., Kanekar, N., & Michałowski, M. J. 2015, MNRAS, 454, L51
Benedict, G. F., Howell, D. A., Jørgensen, I., Kenney, J. D. P., & Smith, B. J. 2002, AJ, 123, 1411
Bigiel, F., Leroy, A., Walter, F., et al. 2008, AJ, 136, 2846
Bose, S., Dong, S., Pastorello, A., et al. 2018, ApJ, 853, 57
Bothwell, M. S., Wagg, J., Cicone, C., et al. 2014, MNRAS, 445, 2599
Bureau, M., & Freeman, K. C. 1999, AJ, 118, 126
Chen, T.-W., Smartt, S. J., Yates, R. M., et al. 2017, MNRAS, 470, 3566
Combes, F., García-Burillo, S., Casasola, V., et al. 2013, A&A, 558, A124
Comerón, S., Knapen, J. H., Beckman, J. E., et al. 2010, MNRAS, 402, 2462
Cooke, J., Sullivan, M., Gal-Yam, A., et al. 2012, Natur, 491, 228
Crowther, P. A., Schnurr, O., Hirschi, R., et al. 2010, MNRAS, 408, 731
Curtin, C., Cooke, J., Moriya, T. J., et al. 2019, ApJS, 241, 17
Decressin, T., Meynet, G., Charbonnel, C., Prantzos, N., & Ekström, S. 2007, A&A, 464, 1029
Elmegreen, B. G. 1994, ApJL, 425, L73
Elmegreen, B. G., Galliano, E., & Alloin, D. 2009, ApJ, 703, 1297
Emsellem, E., Renaud, F., Bournaud, F., et al. 2015, MNRAS, 446, 2468
Gallagher, M. J., Leroy, A. K., Bigiel, F., et al. 2018, ApJ, 858, 90
Gal-Yam, A. 2012, Sci, 337, 927
Gal-Yam, A., & Leonard, D. C. 2009, Natur, 458, 865
Inoue, T., & Fukui, Y. 2013, ApJL, 774, L31
Kennicutt, R. C., Jr. 1998, ApJ, 498, 541
Kewley, L. J., Groves, B., Kauffmann, G., & Heckman, T. 2006, MNRAS, 372, 961
Köhler, K., Langer, N., de Koter, A., et al. 2015, A&A, 573, A71
Langer, N., Norman, C. A., de Koter, A., et al. 2007, A&A, 475, L19
Leitherer, C., Schaerer, D., Goldader, J. D., et al. 1999, ApJS, 123, 3
Leroy, A. K., Bolatto, A. D., Ostriker, E. C., et al. 2015, ApJ, 801, 25
Leroy, A. K., Lee, C., Schruba, A., et al. 2013, ApJL, 769, L12
Lunnan, R., Chornock, R., Berger, E., et al. 2013, ApJ, 771, 97
Lunnan, R., Chornock, R., Berger, E., et al. 2014, ApJ, 787, 138
Lunnan, R., Chornock, R., Berger, E., et al. 2015, ApJ, 804, 90
Maciejewski, W., Teuben, P. J., Sparke, L. S., & Stone, J. M. 2002, MNRAS, 329, 502
McMullin, J. P., Waters, B., Schiebel, D., Young, W., & Golap, K. 2007, in ASP Conf. Ser. 376, Astronomical Data Analysis Software and Systems XVI, ed. R. A. Shaw, F. Hill, & D. J. Bell (San Francisco, CA: ASP), 127
Merrifield, M. R., & Kuijken, K. 1999, A&A, 345, L47
Motte, F., Nguyên Luong, Q., Schneider, N., et al. 2014, A&A, 571, A32
Neill, J. D., Sullivan, M., Gal-Yam, A., et al. 2011, ApJ, 727, 15
Nicholl, M., Berger, E., Margutti, R., et al. 2017, ApJL, 845, L8
Obreschkow, D., Heywood, I., Klöckner, H.-R., & Rawlings, S. 2009, ApJ, 702, 1321
Oke, J. B., Cohen, J. G., Carr, M., et al. 1995, PASP, 107, 375
Pan, T., Loeb, A., & Kasen, D. 2012, MNRAS, 423, 2203
Perley, D. A., Quimby, R. M., Yan, L., et al. 2016, ApJ, 830, 13
Planck Collaboration, Aghanim, N., Akrami, Y., et al. 2018, arXiv:1807.06209
Portegies Zwart, S. F., & van den Heuvel, E. P. J. 2007, Natur, 450, 388
Quimby, R. M., Kulkarni, S. R., Kasliwal, M. M., et al. 2011, Natur, 474, 487
Quimby, R. M., Yuan, F., Akerlof, C., & Wheeler, J. C. 2013, MNRAS, 431, 912
Renaud, F., Bournaud, F., Emsellem, E., et al. 2015, MNRAS, 454, 3299
Roychowdhury, S., Arabsalmani, M., & Kanekar, N. 2019, MNRAS, 485, L93
Sandstrom, K. M., Leroy, A. K., Walter, F., et al. 2013, ApJ, 777, 5
Sheth, K., Vogel, S. N., Regan, M. W., Thornley, M. D., & Teuben, P. J. 2005, ApJ, 632, 217
Singh, R., van de Ven, G., Jahnke, K., et al. 2013, A&A, 558, A43
Smith, N., Li, W., Foley, R. J., et al. 2007, ApJ, 666, 1116
Sun, J., Leroy, A. K., Schruba, A., et al. 2018, ApJ, 860, 172
Takahira, K., Shima, K., Habe, A., & Tasker, E. J. 2018, PASJ, 70, S58
Tan, J. C. 2000, ApJ, 536, 173
van den Heuvel, E. P. J., & Portegies Zwart, S. F. 2013, ApJ, 779, 114